

An Ab Initio Intermolecular Potential Energy Surface for the F₂ Dimer

Mohammad H. Karimi-Jafari and Ali Maghari*

Department of Physical Chemistry, School of Chemistry, University of Tehran, Tehran, Iran

Received: February 19, 2007; In Final Form: May 4, 2007

Two analytical representations for the potential energy surface of the F₂ dimer were constructed on the basis of ab initio calculations up to the fourth-order of Møller–Plesset (MP) perturbation theory. The best estimate of the complete basis set limit of interaction energy was derived for analysis of basis set incompleteness errors. At the MP4/aug-cc-pVTZ level of theory, the most stable structure of the dimer was obtained at $R = 6.82$ au, $\theta_a = 12.9^\circ$, $\theta_b = 76.0^\circ$, and $\varphi = 180^\circ$, with a well depth of $716 \mu E_h$. Two other minima were found for canted and X-shaped configurations with potential energies around -596 and $-629 \mu E_h$, respectively. Hexadecapole moments of monomers play an important role in the anisotropy of interaction energy that is highly R -dependent at intermediate intermolecular distances. The quality of potentials was tested by computing values of the second virial coefficient. The fitted MP4 potential has a more reasonable agreement with experimental values.

1. Introduction

In recent years, high-level quantum mechanical computations have been used to construct numerous accurate potential energy surfaces (PES) for most of the small- and medium-sized molecular species and have been applied successfully in a wide range of applications. However, there have been few high-level studies on the F₂ contained van der Waals complexes.^{1–4} Moreover, molecular fluorine is a highly reactive material, and because of its corrosive nature, there are limited experimental measurements for its molecular^{5–7} and bulk⁸ properties. For such a challenging system, the existence of an accurate intermolecular pair potential will be helpful in future experimental and theoretical studies. To our knowledge, the only ab initio investigation of the F₂ dimer is the work of Noorbala and Sabzyan⁹ that was based on the MP2/6-31G* calculations, for which, at every point on the PES, the monomer bond lengths were left relaxed to be optimized. However, their adopted grid (which included 20 724 points on the PES) did not cover all possible relative orientations of monomers because one of the four intermolecular degrees of freedom was frozen to a fixed value ($\theta_b = 90^\circ$). In any case, their results predicted that the F₂ dimer is thermodynamically stable, and after averaging over dihedral angle between molecules, they obtained an effective PES with a global and a local minimum in parallel and T-shaped orientations, respectively.

Electron correlation contributions to intermolecular interactions have a central role in the structure and the energetics of van der Waals complexes.¹⁰ Electron correlation can commonly be described adequately when one applies a high-level post-Hartree–Fock (HF) method in conjunction with an extended basis set consisting of different types of polarization functions. This is a more difficult task in the case of intermolecular correlation effects because the standard basis sets are mostly optimized for intramolecular properties, and so their application to intermolecular problems usually results in a slow convergence to the complete basis set (CBS) limit. To overcome these

problems, an alternative approach is the use of bond functions located somewhere between monomers. This approach has been widely employed after the works of Tao et al.^{11,12} However, the application of bond functions causes new difficulties. The major issues are the artificial deformation of charge distributions on the monomers and the production of higher-order basis set superposition errors (BSSE) that are uncorrectable via the usual counterpoise procedure.^{13–15} To avoid these deficiencies, Tao and Pan¹¹ proposed two criteria to be satisfied by atom centered basis functions before the addition of bond functions.

Before any comprehensive exploration of the PES, it is necessary to investigate the efficiency of different computational levels to gain a reasonable compromise between precision and computational cost. In the present work, along with a high-level ab initio investigation of the F₂ dimer, analytical four-dimensional representations were obtained for the calculated PES at different levels and were tested against experimental second virial coefficients. Recently, we constructed a new PES for the N₂ dimer¹⁶ utilized to calculate thermophysical properties of nitrogen.¹⁷ Both fluorine and nitrogen molecules are closed shell, linear, and homonuclear, and one might expect that they have similar intermolecular interactions. In our present work, various aspects of the PESs of these systems were compared, and we endeavored to relate the differences between these complexes to their monomer properties.

2. Approach and Methodology

2.1. Grid Points and Computational Levels. The interaction in the F₂–F₂ dimer is described in the body-fixed Jacobi coordinates system,¹⁸ in which the center of mass of molecule a is located at the origin, and the position of the center of mass of molecule b is denoted by pointing vector \mathbf{R} with modulus R and with angles θ_a , θ_b , and $\varphi = \varphi_a - \varphi_b$. The $(R, \theta_a, \theta_b, \varphi)$ notation will be applied to identify different points, curves, or slices of the PES, where R is given in atomic units (au). Before complete exploration of the PES, the efficiency of different computational levels was investigated by some test calculations along the $(7.5, 0, \theta_b, 0)$ slice of the PES for which θ_b varied in steps of 15° . Note that this slice (θ -slice) is equivalent to the

* Corresponding author. Tel and Fax: +98-21-6646-9823, E-mail: maghari@khayam.ut.ac.ir.

(7.5, θ_a , 0, 0) slice because, in the adopted Jacobi coordinates, the PES is symmetric with respect to the $\theta_a = \theta_b$ surface.

After a detailed analysis of the results of different methods and basis sets along the θ -slice was performed, the most efficient computational level was adopted to calculate the PES. All ab initio calculations were performed for 19 unequal distances of R between 4 and 20 au over two different angular grids. The first grid was obtained by varying all angles in steps of 30° and included 37 symmetry unique orientations. Note that the symmetry of the dimer reduces the range of angles to $0 \leq \theta_a \leq \theta_b \leq 90$ and $0 \leq \varphi \leq 180$. Because this grid did not provide a reliable accuracy in the fitting procedure, a second series of calculations was performed over an angular grid with θ_a , $\theta_b = 15, 30$, and 75° and $\varphi = 15, 30$, and 165° . In all calculations, the monomer bond length was kept fixed in its vibrationally averaged experimental value of 2.668 au.⁵

The Møller–Plesset (MP) perturbation theory¹⁹ up to the fourth-order was applied to compute the interaction energy in a supermolecular fashion. According to the counterpoise procedure (cp),²⁰ the cp-corrected interaction energy at each point (R , θ_a , θ_b , φ) is defined in eq 1:

$$U_{\{\text{axb}\}}^{(n)} = E_{\text{ab},\{\text{axb}\}}^{(n)} - E_{\text{a},\{\text{axb}\}}^{(n)} - E_{\text{b},\{\text{axb}\}}^{(n)} \quad (1)$$

where $E_{\text{ab},\{\text{axb}\}}^{(n)}$ and $E_{\text{a},\{\text{axb}\}}^{(n)}$ (or $E_{\text{b},\{\text{axb}\}}^{(n)}$) are dimer and monomer energies, respectively. All of them were obtained at the MP n level of theory utilizing the basis set $\{\text{axb}\}$ of the total complex that includes both the atom centered $\{\text{a}\}$ and $\{\text{b}\}$ sets of monomers and the non-atom centered set $\{\text{x}\}$ of bond functions. The calculations reported in this work employ the correlation consistent cc-pVXZ, and their augmented version aug-cc-pVXZ, sets of Dunning and co-workers,^{21,22} (XZ and aXZ (X = D, T, Q, 5, and 6), respectively). Because of computational limitations, all h and i functions were eliminated from 5Z, a5Z, 6Z, and a6Z sets, and the resulting subsets will be denoted as 5Z1, a5Z1, 6Z2, and a6Z2, respectively. The 3s3p2d1f set of bond functions (+b) recommended by Tao and Pan¹¹ was utilized in conjunction with aXZ atom centered basis sets. All bond functions were located at the middle of intermolecular pointing vector \mathbf{R} . The ab initio calculations reported in this paper were carried out using the PC GAMESS suite of programs.^{23,24}

2.2. Global Representation of the PES. To obtain an analytic representation of the F_2 – F_2 potential, the interaction energies calculated at each value of R were fitted to the spherical expansion shown in eq 2:^{25,26}

$$U(R, \theta_a, \theta_b, \varphi) = \sum_{L_a, L_b, L} V_{L_a, L_b, L}(R) A_{L_a, L_b, L}(\theta_a, \theta_b, \varphi) \quad (2)$$

where L_a , $L_b = 0, 1, 2, \dots$ and $|L_a - L_b| \leq L \leq L_a + L_b$. The symmetry of the F_2 dimer leads to the relation $V_{L_a, L_b, L} = V_{L_b, L_a, L}$ between expansion coefficients, and only even moments appear in eq 2. Angular basis functions ($A_{L_a, L_b, L}$) are shown in eq 3:

$$A_{L_a, L_b, L}(\theta_a, \theta_b, \varphi) = \sum_{M=0}^{\min(L_a, L_b)} (-1)^M (2 - \delta_{M,0}) \langle L_a, M; L_b, -M | L, 0 \rangle \times \left[\frac{(L_a - M)!(L_b - M)!}{(L_a + M)!(L_b + M)!} \right]^{1/2} \times P_{L_a}^M(\cos \theta_a) P_{L_b}^M(\cos \theta_b) \cos(M\varphi) \quad (3)$$

where $P_L^M(\cos \theta)$ stands for the associated Legendre polynomials, and $\langle L_a, M; L_b, -M | L, 0 \rangle$ is the Clebsch–Gordan coefficient.

The expansion coefficients $V_{L_a, L_b, L}(R)$ were evaluated using a weighted linear least-squares procedure. The most important concern in the adopted fitting procedure was to obtain an accurate representation of the PES in its bond region ($U < 0$). Consequently, at each value of R all ab initio energies $\{U_i\}$ were weighted using a nonuniform weight function of the form $(1 - (U_i - U_{\min})^2)^{-1}$. In this step, a reliable accuracy was obtained using a set of 24 $V_{L_a, L_b, L}$ coefficients that covers all 18 terms up to $L_a = 6$ and $L_b = 2$ and another six terms with $L_a + L_b = L$ up to $L_a = 8$ and $L_b = 6$.

The full potential was obtained by fitting the resulted $V_{L_a, L_b, L}$ coefficients over the grid of R points. Following Vissers et al.,²⁷ the long-range part of $V_{L_a, L_b, L}$ was fitted by a two-parameter single-term functional of the form shown in eq 4.

$$V_{L_a, L_b, L}^{LR}(R) = \frac{c_{L_a, L_b, L}}{R^{\nu_{L_a, L_b, L}}} \quad (4)$$

These long-range terms were damped by a Tang–Toennies²⁸ damping function, shown in eq 5.

$$F(R; n, \alpha) = 1 - \exp(-\alpha R) \sum_{k=0}^n \frac{(\alpha R)^k}{k!} \quad (5)$$

The resulting terms were subtracted from $V_{L_a, L_b, L}$ to obtain the short-range contributions as shown in eq 6:

$$V_{L_a, L_b, L}^{SR}(R) = V_{L_a, L_b, L}(R) - F(R; n_{L_a, L_b, L}, \alpha_{L_a, L_b, L}) \frac{c_{L_a, L_b, L}}{R^{\nu_{L_a, L_b, L}}} \quad (6)$$

where $n_{L_a, L_b, L}$ was taken to be the integer closest to $\nu_{L_a, L_b, L}$. The resulting short-range contributions were then fitted to the form shown in eq 7:

$$V_{L_a, L_b, L}^{SR}(R) = \exp(-\alpha_{L_a, L_b, L} R) \sum_{k=0}^{k_{\max}} d_{L_a, L_b, L} R^k \quad (7)$$

where k_{\max} is a proper integer between 2 and 6. The parameters $\alpha_{L_a, L_b, L}$, which appeared both in the damping function and in the short-range functional form, were obtained by an iterative procedure started with an initial guess for $\alpha_{L_a, L_b, L}$ in eq 6. It must be noted that certain $\{L_a, L_b, L\}$ combinations do not contribute to the long-range part of $V_{L_a, L_b, L}$. In these cases, the long-range fit of eq 4 was not possible; consequently, the corresponding $c_{L_a, L_b, L}$ parameters were set equal to zero.

In an alternative approach for global representation of the PES and after the least-squares fitting of eq 2 was performed, radial fitting of the $V_{L_a, L_b, L}$ terms was replaced by a piecewise polynomial interpolation of their values along the R grid. This fitting-interpolating surface, which is accurate to within the order of errors introduced in the angular fitting step, was applied to trace the behavior of the above-mentioned full-fitting surface and to remove its unexpected errors by refinement of radial parameters.

3. Results and Discussions

3.1. Monomer Properties. Before proceeding with the calculation of interaction energies, we investigated some monomer properties that are relevant to intermolecular forces. Quadrupole (Θ) and hexadecapole (Φ) moments and static polarizability (α) of the F_2 molecule were calculated with both XZ and aXZ basis sets at HF and MP2 levels of theory. The corresponding results are collected in Table 1, in which the mean

TABLE 1: Quadrupole (Θ), Hexadecapole (Φ), Mean ($\bar{\alpha}$) and Anisotropic ($\Delta\alpha$) Polarizability of the F₂ Molecule Obtained with Different Basis Sets at HF and MP2 Levels of Theory^a

basis set	Θ		Φ		$\bar{\alpha}$		$\Delta\alpha$	
	HF	MP2	HF	MP2	HF	MP2	HF	MP2
TZ	0.541	0.737	11.52	13.05	6.267	5.053	10.274	6.527
QZ	0.520	0.750	11.57	13.27	7.167	6.115	9.857	6.091
5Z1	0.500	0.749	11.63	13.54	7.716	6.844	9.639	5.848
aTZ	0.534	0.784	12.10	14.03	8.418	7.869	9.088	5.108
aQZ	0.511	0.770	12.03	13.89	8.563	8.095	9.053	5.011
a5Z1	0.495	0.756	11.86	13.73	8.577	8.140	9.072	5.022

^a All values are in atomic units (au).

polarizability ($\bar{\alpha}$) and its anisotropy ($\Delta\alpha$) are defined as $(\alpha_{xx} + \alpha_{yy} + \alpha_{zz})/3$ and $\alpha_{zz} - (\alpha_{xx} + \alpha_{yy})/2$, respectively.¹⁸ Different components of the polarizability tensor were obtained by the finite field method.^{29,30}

In agreement with the well-known crucial role of diffuse functions for accurate description of intermolecular interactions, their presence is important for rapid convergence of multipole moments and polarizabilities to the CBS limit. In comparison with the N₂ molecule,¹⁶ an important feature of the F₂ molecule is its larger hexadecapole and smaller quadrupole moments. This fact has important consequences for anisotropic aspects of the PES that will be discussed later.

As can be seen in Table 1, most of the calculated multipole moments with the aXZ and the XZ basis sets converge to the CBS limit from opposite sides. Therefore, the CBS limit is bounded between aXZ and XZ values, and the simple arithmetic mean of a5Z1 and 5Z1 values can be used to estimate the CBS limit of quadrupole and hexadecapole moments. Accordingly, we have obtained 0.49 and 11.75 au for the CBS limits of HF quadrupole and hexadecapole moments and 0.75 and 13.63 au for the CBS limits of MP2 quadrupole and hexadecapole moments, respectively. Polarizability cannot be estimated in a similar manner because both XZ and aXZ values converge to the CBS limit from the same side. However, the small difference between the aQZ and the a5Z1 values (which is less than 0.5%) shows that a5Z1 polarizabilities are nearly converged to the CBS limit. It is also observed that the correlation contribution to multipole moments and to the polarizabilities of monomers is nearly the same for different aXZ basis sets and seems to be converging more rapidly than the HF contribution.

3.2. Benchmark Calculations along the θ -Slice. The estimated CBS limit of MP2 and MP4 interaction energies and those obtained with aTZ and aTZ+b basis sets along the θ -slice are shown in Figure 1. For the most stable point of this slice, the corresponding numerical values and those of other basis sets are summarized in Table 2. Different strategies were employed to estimate the CBS limit of HF and the correlation components of interaction energy, because they have different convergence behaviors. Moreover, considering the computational cost of these methods, it is possible to obtain HF values with more extended basis sets than with those applied in calculation of correlation corrections.

As can be seen in Table 2 by the comparison of a5Z1 with a6Z2, the values of the HF interaction energy demonstrate that the a6Z2 values are nearly converged. Moreover, the cp-corrected and uncorrected values of interaction energy and its components converge to the CBS limit from opposite sides, and the magnitude of BSSE for the HF/a6Z2 energy is, on average, less than 2 μE_h along the θ -slice. According to these facts, a simple average of the cp-corrected and uncorrected values is expected to be within 1 μE_h of the CBS limit. This simple

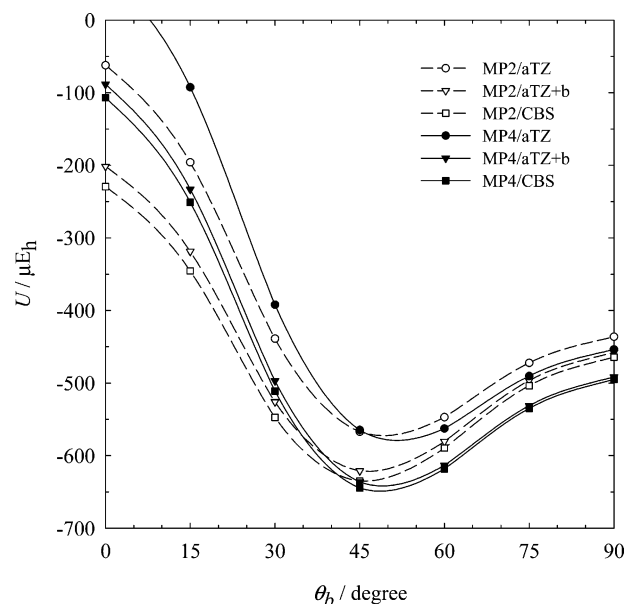


Figure 1. Comparison of MP2 and MP4 interaction energies obtained with aTZ and aTZ+b basis sets with the estimated CBS values along the (7.5, 0, θ_b , 0) slice of the PES.

average was adopted as our best estimate of the HF limit of interaction energy. In the case of correlation components of interaction energy, the values obtained with a5Z1+b were chosen as our best estimates of the CBS limit. Comparison of aQZ+b with a5Z1+b values in Table 2 demonstrates that the correlation corrections of interaction energy is nearly converged with respect to {spdfg} basis functions, and the remaining errors due to higher polarization functions are minor (as expected), because the bond functions recover their contributions.

A well-known feature of MP perturbation theory is its problematic convergence, in some systems, due to exaggeration of correlations at some levels of MP. This behavior is expected to occur at situations with a high degree of electron clustering.³¹ In the F₂-F₂ system, the convergence pattern of the MP series for total energy of the complex is similar to that of monomers. In both cases, there are oscillations in which $E^{\text{HF}} > E^{(3)} > E^{(2)} > E^{(4)}$. This trend seems to be independent of the selected basis set and the geometry of the complex. In the case of interaction energies, the noticeable fact that could be found in Figure 1 is the angular dependence of the MP convergence pattern. In most configurations, MP interaction energies have the same oscillatory behavior as those of total energies, but in configurations near to (R, 0, 0, 0), $U^{(2)}$ becomes more stable than $U^{(4)}$.

3.3. Role of Electrostatic Interactions on the Shape of the PES. As is expected from the physical nature of interaction in this system,¹⁸ the (R, 0, 0, 0) orientation is the most repulsive one along the θ -slice, because the short-range exchange and the overlap repulsions are maximized for the linear structure of the complex. Furthermore, the electrostatic components of interaction have their maximum repulsive values at this orientation. The main difference between this complex and other similar systems, such as the N₂ dimer, corresponds to the location of the most attractive orientation in Figure 1. This characteristic structural feature is controlled by the relative importance and anisotropic behavior of dispersion and electrostatic attractions and by the anisotropic nature of decay rate of short-range repulsions.

To examine anisotropy and the importance of multipole–multipole interactions, the electrostatic components of interaction

TABLE 2: Basis Set Convergence of HF, MP2, and MP4 Interaction Energies and Their Correlation Contributions at the (7.5, 0, 45, 0) Configuration^a

basis set	U^{HF}	$U_{\text{correlation}}^{(2)}$	$U_{\text{correlation}}^{(4)}$	$U^{(2)}$	$U^{(4)}$
aTZ	386 (-107)	-953 (-148)	-951 (-186)	-567	-565
aQZ	399 (-60)	-994 (-92)	-1000 (-89)	-595	-601
a5Z1	396 (-10)	-1013 (-53)	-1020 (-42)	-616	-624
a6Z2	396 (-2)				
aTZ+b	398 (-1113)	-1019 (-2194)	-1035 (-2422)	-621	-636
aQZ+b	396 (-316)	-1028 (-901)	-1039 (-818)	-632	-643
a5Z1+b	396 (-30)	-1030 (-407)	-1039 (-323)	-634	-644
estimated CBS	395	-1030	-1039	-635	-645

^a Values in parentheses are cp-corrected BSSEs. All energies are in μE_h .

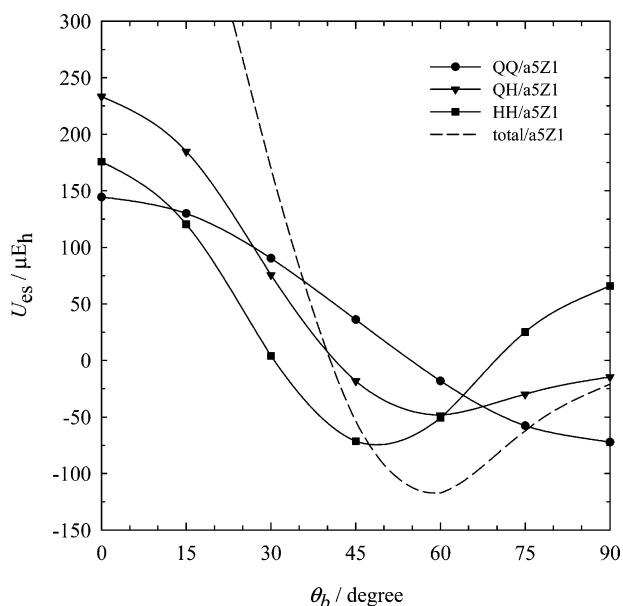


Figure 2. Different components of the electrostatic interaction energy, and its total value along the (7.5, 0, θ_b , 0) slice of the PES obtained at the MP2/a5Z1 level of theory.

energy along the θ -slice are shown in Figure 2. These contributions are defined via a multipole expansion of the form shown in eq 8:

$$U_{\text{es}}(R, \theta_a, \theta_b, \varphi) = \sum_{L_a, L_b, L} \delta_{L_a+L_b, L} \frac{M_{L_a} M_{L_b} B_{L_a, L_b, L}(\theta_a, \theta_b, \varphi)}{R^{L_a+L_b+1}} \quad (8)$$

where M_{L_a} and M_{L_b} are permanent multipole moments of molecules a and b, which have nonzero values only for $L_a, L_b \geq 2$ ($M_2 \equiv \Theta$, $M_4 \equiv \Phi$, ...). The functions $B_{L_a, L_b, L}$ which are responsible for the angular dependence of interaction, are related to $A_{L_a, L_b, L}$ in eq 2 with the same indices. The first three terms, which appeared in eq 8, are quadrupole–quadrupole (QQ), quadrupole–hexadecapole (QH) and hexadecapole–hexadecapole (HH) interactions. As can be seen in Figure 2, the minimum of the leading QQ term along the θ -slice corresponds to (R, 0, 90, 0) (the T-shaped orientation), but those of the QH and the HH contributions occur at $\theta_b = 59.5^\circ$ and 49° , respectively. For the total electrostatic interaction, the shape of the curve and the location of its minimum depend on the relative magnitude of quadrupole and hexadecapole moments of diatomic monomers. In comparison with the N_2 dimer,¹⁶ the minimum of the total electrostatic interaction of the F_2 dimer is shifted to smaller θ_b angles as a result of overall larger hexadecapole and smaller quadrupole moments.

Comparison between Figures 1 and 2 suggests that the anisotropy of total interaction energy at correlated levels of

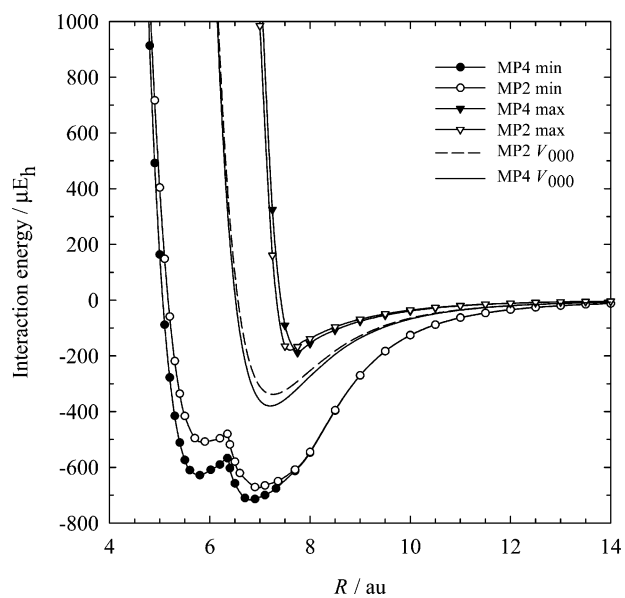


Figure 3. Radial dependence of the isotropic part of fitted potentials and the corresponding minimized (min) and maximized (max) values over angular coordinates.

theory is controlled by the anisotropy of electrostatic component of interaction, and the latter is dominantly affected by the terms containing the hexadecapole moment in the multipole expansion. It is important to note that the order of magnitude of the overlap repulsions and of the dispersion attractions is usually larger than that of the electrostatic interactions,¹⁰ but at an intermediate range they compensate for each other at correlated levels of theory, and the shape of the PES becomes more sensitive to the anisotropy of electrostatic components. At the HF level of theory, the dispersion contributions are absent, and the overall shape of the PES, which monotonically decreases along the θ -slice, is determined by strong overlap repulsions and the anisotropy of electrostatic components is effaced. At other intermolecular distances, the location of the minimum in Figure 1 will shift toward the end of the slice, because (i) at larger values of R the minimum of electrostatic interaction moves to the (R, 0, 90, 0) orientation, because the QQ term, which appeared in eq 8, becomes more and more dominant; and (ii) at smaller values of R , despite the fact that the electrostatic interaction becomes more attractive around intermediate values of θ_b , the rapid increase of overlap repulsions efface all electrostatic components in favor of the (R, 0, 90, 0) orientation.

3.4. Structural Features of the Fitted PES. According to the above-mentioned results along the θ -slice, the best compromise between accuracy and computational cost was achieved by the aTZ+b basis set. Consequently, this basis set was utilized to calculate the interaction energy over the selected grid up to the fourth-order of MP, and then both the resulting MP2 and

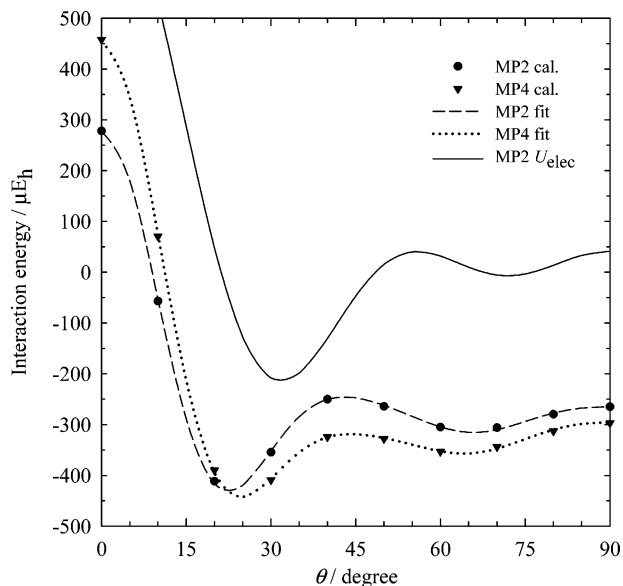


Figure 4. Angular dependence of fitted potentials and electrostatic interactions along the $(7.2, \theta, \theta, 0)$ slice of the PES in comparison with calculated points that were not included in the fit.

the MP4 ab initio points were fitted. The analytical representation of potential is sufficiently flexible that, despite the large number of radial grid points used, the overall agreement of the fit is very good. In the bond region of the potential ($U < 0$), discrepancies between the fitted values and the calculated ab initio points are smaller than $4.5 \mu E_h$, with a root-mean-square error of $0.7 \mu E_h$. At more repulsive energies ($U > 300 \mu E_h$) the largest relative error is $\approx 4.2\%$, with an average error of $\approx 0.6\%$. Notably, the fitted PES is accurate at the most stable structures. Its relative error at the well depth of investigated orientations is, on average, less than $\approx 0.2\%$, with a maximum error of $\approx 1.3\%$.

In Figure 3, the radial dependence of the isotropic V_{000} part of the fitted MP2 and MP4 potentials are compared with each other. Note that in eq 2, $A_{000} = 1$. This figure also contains the optimized energy curves obtained at each value of R by minimization and maximization of potentials over all angular coordinates. Both the MP2 and the MP4 potentials show the same double-well structure over the minimized energy curve, but the former is shallower, especially around the local minimum located at smaller R . The same thing can be said about the isotropic part of the potentials. At distances smaller than 6 au, all minimized and maximized energies correspond to the $(90, 90, 90)$ and $(0, 0, 0)$ orientations, respectively. In agreement with our previous discussion about the oscillatory behavior of MP series, comparison of the maximized energy curves shows that the MP2 potential is less repulsive than the MP4 one at short range.

Exploration of the fitted surfaces demonstrated that some of the most important characteristic points on the PES of the F₂ dimer are located at the $\theta_a = \theta_b$ surface. Thus, some further ab initio calculations were performed to check the reliability of the fitted potentials over this surface. In Figure 4, the $(7.2, \theta, \theta, 0)$ slice of fitted surfaces is compared with ab initio points, none of which were included in the fit. The PES oscillates along the $\theta_a = \theta_b$ surface. This feature remains valid at all intermediate distances, and as a result, the PES shows two saddle points and a local minimum with $\theta_a = \theta_b$ and $\varphi = 0$. To further emphasize the role of electrostatic forces on the shape of the PES of the F₂ dimer, the corresponding MP2 values of total electrostatic interactions are plotted in Figure 4. It must be noted that the

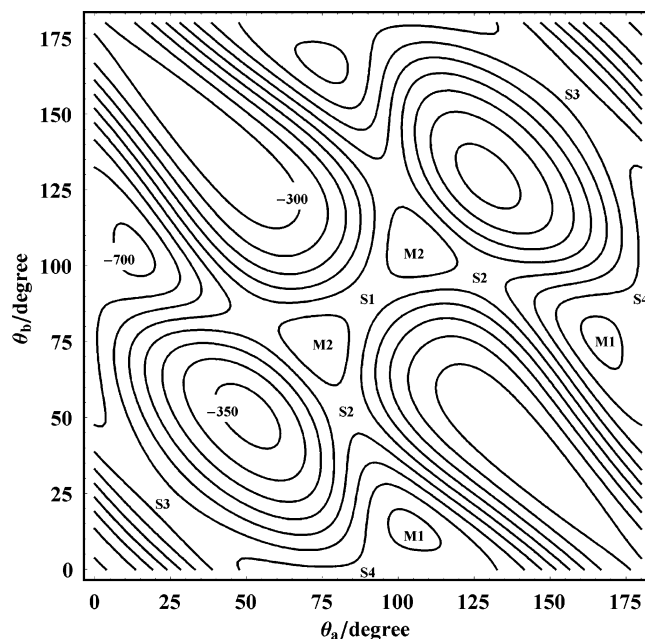


Figure 5. A cut through the fitted MP4 potential for $\varphi = 0$ and R -values that minimize interaction energy for the given angles. See Table 3 for a description of minima and saddle points. The contours are separated by $50 \mu E_h$.

individual QQ term has a single minimum along this slice, and the double-well structure of the curves in Figure 4 originates from similar structures of QH and HH interactions.

The oscillatory behavior of the PES along the $\theta_a = \theta_b$ surface can be seen more obviously in Figure 5. This figure is a cut through the full MP4 surface for $\varphi = 0$ and for R values that minimize the interaction energy in each (θ_a, θ_b) point. By extending the range of θ_a and θ_b to 180° , this figure also contains all planar structures with $\varphi = 180^\circ$. To interpret this figure, note the following relation (eq 9):

$$U(R, \theta_a, \theta_b, \varphi) = U(R, \theta_a, \pi - \theta_b, \pi - \varphi) = U(R, \pi - \theta_a, \theta_b, \pi - \varphi) = U(R, \pi - \theta_a, \pi - \theta_b, \varphi) \quad (9)$$

The same minimized 2D cross-section of the PES for $\varphi = 90^\circ$ is depicted in Figure 6. The characteristic points visible in these figures are listed in Table 3. The global minimum of the PES (M1 in Figure 5 and Table 3) is the $(6.82, 12.9, 76.0, 180)$ configuration with a well depth of $716 \mu E_h$. Remember that this configuration is equivalent to $(6.82, 104.0, 12.9, 0)$. Also, there are two other minima with well depths of 596 and $629 \mu E_h$. The former (M2 in Figure 5) is a planar structure with $\theta_a = \theta_b = 73^\circ$, and the latter (M3 in Figure 6) that is located at shorter distances is a crossed structure with $\theta_a = \theta_b = \varphi = 90^\circ$. As can be seen in Figure 5, the global minimum M1 and the local minimum M2 are connected via a saddle point (S2). Relative to M1, the barrier for this motion is around $180 \mu E_h$. Energetically, there is a more favorable motion with a barrier around $60 \mu E_h$ that passes the T-shaped structure (S4) in Figure 5. This saddle point connects the global minimum to a symmetrically equivalent structure on the PES. For local minimum M2, a similar motion to its symmetrically equivalent structure has a barrier around $70 \mu E_h$ and is associated with the parallel structure (S1 in Figure 5).

3.5. Second Virial Coefficient. As a pure two body interaction property, the second virial coefficient $B(T)$ was calculated to give a first, simple test of the quality of the fitted MP2 and

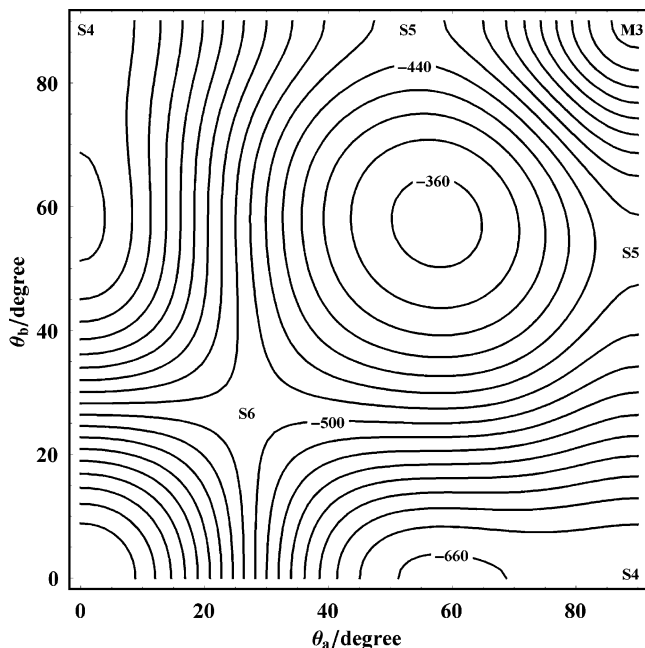


Figure 6. Same as Figure 5 for $\varphi = 90$. The contours are separated by $20 \mu E_h$.

TABLE 3: Position of the Minima (M) and Saddle Points (S) on the Fitted MP4 PES and Their Associated Interaction Energies^a

minima and saddle points	R	θ_a	θ_b	φ	$U^{(4)}$	$U^{(2)}$
M1	6.82	12.9	76.0	180	-716.3	-657.4
M2	6.04	73.7	73.7	0	-596.2	-493.6
M3	5.76	90	90	90	-629.1	-504.4
S1	6.06	90	90	0	-525.4	-431.6
S2	6.41	82.6	52.8	0	-535.1	-452.6
S3	7.61	22.6	22.6	0	-616.4	-609.1
S4	6.78	0	90	0	-658.3	-591.5
S5	6.56	53.3	90	90	-455.1	-372.5
S6	7.67	27.2	27.2	90	-492.5	-486.3

^a All distances are in au, angles are in degrees, and energies are in μE_h .

MP4 potentials. The value of $B(T)$ for a given temperature T was calculated from eq 10:

$$B(T) = \frac{N_A}{4} \int_0^{2\pi} d\varphi \int_0^\pi \int_0^\pi \sin \theta_a \sin \theta_b d\theta_a d\theta_b \int_0^\infty r^2 dr \times \left\{ 1 - \exp\left(\frac{-U(R, \theta_a, \theta_b, \varphi)}{k_B T}\right) \right\} \quad (10)$$

in which k_B and N_A are Boltzman's and Avogadro's constants, respectively. We used a multidimensional adaptive quadrature method with an absolute error estimate of better than $0.05 \text{ cm}^3 \cdot \text{mol}^{-1}$. The stability of the results was checked against the variation of the integration parameters. The quantum correction to $B(T)$ was expected to be small and was ignored.

In Figure 7, calculated second virial coefficients are compared with experimental data.^{32,33} Available experimental data of $B(T)$ are lower than the Boyle temperature, and those of ref 33 seem to be more accurate. At all temperatures, the MP4 potential exhibits a more reasonable agreement with experiment than the MP2 one. Differences between the MP2 and the MP4 values of $B(T)$ are consistent with the shallowness of the MP2 potential. At the lowest temperature, the uncertainty of the measurements reported in ref 33 is $40 \text{ cm}^3 \cdot \text{mol}^{-1}$, and the MP4 value of $B(T)$

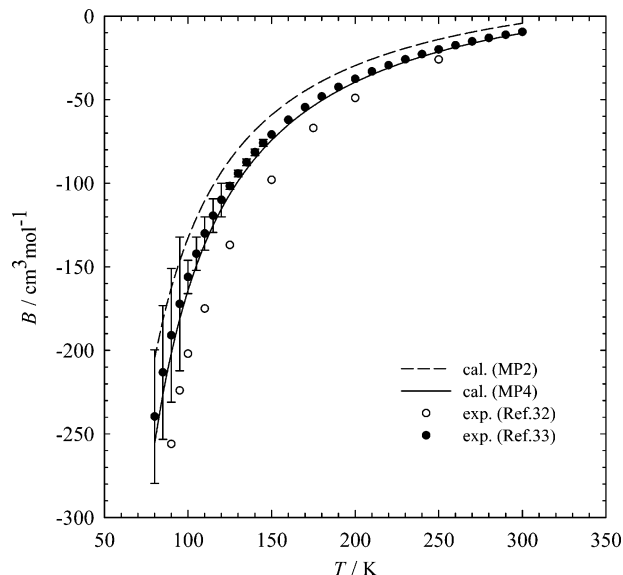


Figure 7. Calculated second virial coefficients in comparison with experimental results. See refs 32 and 33.

is $16.4 \text{ cm}^3 \cdot \text{mol}^{-1}$ ($\approx 6.8\%$) lower than the experimental result. At higher temperatures deviations decreased, but for $T > 120 \text{ K}$ they are larger than the experimental uncertainty.

4. Conclusions

In the present work, after a detailed analysis of various ab initio derived interaction energies along an angular slice of the PES, the aTZ+b basis set was utilized for calculation of the PES up to the fourth-order of MP perturbation theory. Basis set convergence of monomer properties were analyzed, and MP2 values of 0.75, 13.63, and 8.14 au were obtained for quadrupole, hexadecapole, and the mean polarizability of the F_2 molecule near the CBS limit. Best estimates of the CBS limit of interaction energy were derived and were used for analysis of the basis set incompleteness errors at different computational levels. Basis set incompleteness error of the MP4/aTZ+b interaction energies was estimated to be, on average, less than 3%. It was found that the MP2 method is unable to reproduce the anisotropy of the PES accurately, even near the CBS limit. Especially at short range and close to the $(R, 0, 0, 0)$ orientation, the relative stability of the configurations obtained with MP2 is completely different from those of MP4. Examination of the different components of the electrostatic contribution of the interaction energy demonstrated that the hexadecapole moments of molecules play an important role in the anisotropy of electrostatic and total interaction energy of the F_2 dimer at intermediate intermolecular distances.

Both the MP2 and the MP4 interaction energies were calculated at 1387 points on the PES and were used to construct analytical potentials with a spherical expansion functional form. The global minimum of the fitted MP4 PES was found to be the $(6.82, 12.9, 76, 180)$ configuration with the well depth of $716 \mu E_h$. Two other minima were found at the $(6.04, 73.7, 73.7, 0)$ and the $(5.76, 90, 90, 90)$ configurations with potential energies around -596 and $-629 \mu E_h$, respectively. Comparison of the results obtained for the F_2 dimer in the present study with those of the N_2 dimer¹⁶ demonstrated that the anisotropy of the PESs of these systems at short range is similar, but it becomes completely different at intermediate and large intermolecular distances as a result of differences between the multipole moments of these molecules. Values of the classical second virial coefficient calculated with fitted MP2 and MP4

potentials were compared with experimental data. The MP4 potential exhibits a more reasonable agreement with experimental data.

Acknowledgment. We are thankful to the Research Council of University of Tehran for their support of this work. The authors thank Dr. Reza Hoseinnezhad for his helpful suggestions.

References and Notes

- (1) Chan, K. W.; Power, T. D.; Jai-nhuknan, J.; Cybulski, S. M. *J. Chem. Phys.* **1999**, *110*, 860.
- (2) Karpfen, A. *Chem. Phys. Lett.* **1999**, *299*, 493.
- (3) Karpfen, A. *Chem. Phys. Lett.* **2000**, *316*, 483.
- (4) Lourderaj, U.; Sathyamurthy, N. *Chem. Phys.* **2005**, *308*, 277.
- (5) Colbourn, E. A.; Dagenais, M.; Douglas, A. E.; Raymonda, J. W. *Can. J. Phys.* **1976**, *54*, 1343.
- (6) Schwentner, N.; Apkarian, V. A. *Chem. Phys. Lett.* **1989**, *154*, 413.
- (7) Bressler, C.; Lawrence, W. G.; Schwentner, N. *J. Chem. Phys.* **1996**, *105*, 1318.
- (8) Hanley, H. J. M.; Prydz, R. *J. Phys. Chem. Ref. Data* **1972**, *1*, 1101.
- (9) Noorbala, M. R.; Sabzyan, H. *Theochem* **2004**, *678*, 67.
- (10) Chalasinski, G.; Szczesniak, M. M. *Chem. Rev.* **1994**, *94*, 1723.
- (11) Tao, F.-M.; Pan, Y.-K. *J. Chem. Phys.* **1992**, *97*, 4989.
- (12) Tao, F.-M. *J. Chem. Phys.* **1993**, *98*, 3049.
- (13) Cybulski, S. M. *Chem. Phys. Lett.* **1994**, *228*, 451.
- (14) Kukawska-Tarnawska, B.; Chalasinski, G.; Olszewski, K. *J. Chem. Phys.* **1994**, *101*, 4964.
- (15) Burcl, R.; Chalasinski, G.; Bukowski, R.; Szczesniak, M. M. *J. Chem. Phys.* **1995**, *103*, 1498.
- (16) Karimi-Jafari, M. H.; Maghari, A.; Shahbazian, S. *Chem. Phys.* **2005**, *314*, 249.
- (17) Karimi-Jafari, M. H.; Maghari, A. *Int. J. Thermophysics* **2006**, *27*, 1449.
- (18) Stone, A. J. *The Theory of Intermolecular Forces*; Oxford University Press: New York, 1996.
- (19) Møller, C.; Plesset, M. S. *Phys. Rev.* **1934**, *46*, 618.
- (20) Boys, S. F.; Bernardi, F. *Mol. Phys.* **1970**, *19*, 553.
- (21) Dunning, T. H., Jr. *J. Chem. Phys.* **1989**, *90*, 1007.
- (22) Woon, D. E.; Dunning, T. H., Jr. *J. Chem. Phys.* **1993**, *98*, 1358.
- (23) Schmidt, M. W.; Baldridge, K. K.; Boatz, J. A.; Elebert, S. T.; Gordon, M. S.; Jensen, J. H.; Koseki, S.; Matsunaga, N.; Nguyen, K.; Su, S. J.; Windus, T. L.; Dupuis, M.; Montgomery, J. A. *J. Comput. Chem.* **1993**, *14*, 1347.
- (24) Granovsky, A. A. PC GAMESS version 7.0, <http://classic-chem.msu.su/gran/gamess/index.html>.
- (25) Gray, G. C.; Gubbins, K. E. *Theory of Molecular Fluids*; Clarendon Press: Oxford, 1984.
- (26) van der Avoird, A.; Wormer, P. E. S.; Szalewicz, R. *Chem. Rev.* **1994**, *94*, 1931.
- (27) Vissers, G. W. M.; Wormer, P. E. S.; van der Avoird, A. *Phys. Chem. Chem. Phys.* **2003**, *5*, 4767.
- (28) Tang, K. T.; Toennies, J. P. *J. Chem. Phys.* **1984**, *80*, 3726.
- (29) Gready, J. E.; Bacskey, G. B.; Hush, N. S. *Chem. Phys.* **1977**, *22*, 141.
- (30) Kurtz, H. A.; Stewart, J. J. P.; Dieter, K. M. *J. Comput. Chem.* **1990**, *11*, 82.
- (31) Cremer, D.; He, Z. *J. Phys. Chem.* **1996**, *100*, 6173.
- (32) White, D.; Hu, J.-H.; Johnston, H. L. *J. Chem. Phys.* **1953**, *21*, 1149.
- (33) Prydz, R.; Stratz, G. C. *J. Res. Natl. Bur. Stand.* **1970**, *74A*, 747.